Nucleation Kinetics of Proeutectoid Ferrite at Austenite Grain Boundaries in Fe-C-X Alloys

M. ENOMOTO and H. I. AARONSON

The nucleation kinetics of proeutectoid ferrite allotriomorphs at austenite grain boundaries in Fe-0.5 at. pct C-3 at. pct X alloys, where X is successively Mn, Ni, Co, and Si and in an Fe-0.8 at. pct C-2.5 at. pct Mo alloy have been measured using previously developed experimental techniques. The results were analyzed in terms of the influence of substitutional alloying elements upon the volume free energy change and upon the energies of austenite grain boundaries and nucleus:matrix boundaries. Classical nucleation theory was employed in conjunction with the pillbox model of the critical nucleus applied during the predecessor study of ferrite nucleation kinetics at grain boundaries in Fe-C alloys. The free energy change associated with nucleation was evaluated from both the Hillert-Staffanson and the Central Atoms Models of interstitial-substitutional solid solutions. The grain boundary concentrations of X determined with a Scanning Auger Microprobe were utilized to calculate the reduction in the austenite grain boundary energy produced by the segregation of alloying elements. Analysis of these data in terms of nucleation theory indicates that much of the influence of X upon ferrite nucleation rate derives from effects upon the volume-free energy change, *i.e.*, upon alterations in the path of the $\gamma/(\alpha + \gamma)$ phase boundary. Additional effects arise from reductions in austenite grain boundary energy, with austenite-forming alloying elements being more effective in this regard than ferrite-formers. By difference, the remaining influence of the alloy elements studied evidently results from their ability to diminish the energies of the austenite:ferrite boundaries enclosing the critical nucleus. The role of nucleation kinetics in the formation of a bay in the TTT diagram of Fe-C-Mo alloys is also considered.

I. INTRODUCTION

SEVERAL studies have been reported on the heterogeneous nucleation kinetics of proeutectoid ferrite at austenite grain boundaries in alloy steels.[1-4] However, most of these studies are seriously compromised by inadequate methods of making the nucleation rate measurements, by analyses based on semi-quantitative rate equations, and by ancillary parameter data not accurately applicable to the complex commercial-type steels employed.

In the recently-completed study of the nucleation kinetics of grain boundary allotriomorphs of proeutectoid ferrite at austenite grain boundaries in high-purity Fe-C alloys by Lange *et al.*,[5] several important improvements in the experimental techniques for conducting such measurements were made: (1) nucleation at austenite grain faces was distinguished from that at grain edges by careful delineation of the former austenite grain boundaries; (2) the Schwartz-Saltykov analysis[6,7] was used to convert the number and the size distribution of ferrite crystals on the plane of polish to the actual size distribution and the total number per unit area of untransformed and compositionally unaffected (hereafter simply unreacted) grain boundary; (3) a correction was made for the effects of the carbon diffusion field surrounding previously nucleated ferrite allotriomorphs on subsequent nucleation at the grain boundaries.

The measured nucleation rates were shown to be far too rapid to be explained by critical nuclei based upon high interfacial energy spherical caps. Pillbox-type nuclei of the type shown in Figure 1 were accordingly proposed. The model of Figure 1(a) is taken to have very low energy edges and low energy broad faces. The models of Figures 1(b) and 1(c) replace one low energy, coherent broad face with a high energy, disordered-type spherical cap; this is permissible

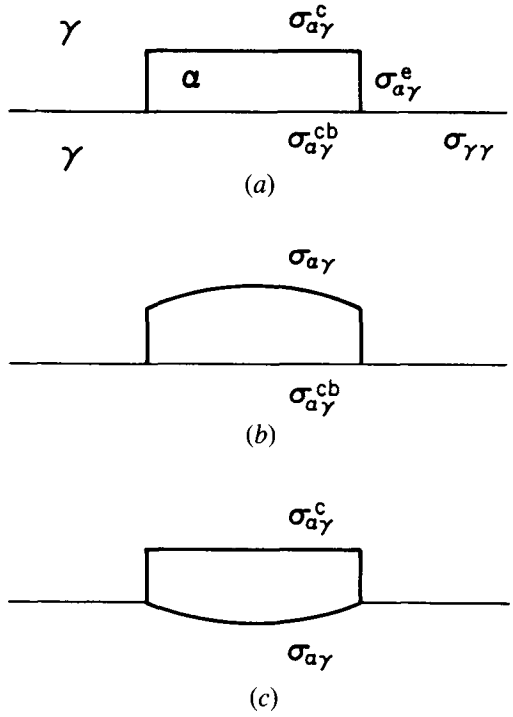

Fig. 1—Three variants of pillbox critical nucleus model:[5] (*a*) both top and bottom surfaces are low energy $\alpha:\gamma$ interfaces; (*b*) top broad surface and (*c*) bottom surface are high energy $\alpha:\gamma$ interfaces.

M. ENOMOTO, formerly Graduate Student, Department of Metallurgical Engineering and Materials Science, Carnegie-Mellon University, is Senior Researcher, Tsukuba Laboratories, National Research Institute for Metals, 1-2-1 Sengen, Sakura-Mura, Niihari-Gun, Ibaraki 305, Japan. H. I. AARONSON is R. F. Mehl Professor, Department of Metallurgical Engineering and Materials Science, Carnegie-Mellon University, Pittsburgh, PA 15213.

Manuscript submitted September 11, 1985.

when the other broad face has a sufficiently low energy; these two models yield kinetics little different from that of Figure 1(a). Although the latter two are crystallographically less restrictive, nonetheless accurate parallelism of a low energy broad face to one of the conjugate planes forming the austenite grain boundary is required, thus providing a basis for sharply restricting the proportion of the grain boundary area at which nucleation can take place — without even considering the structure of the grain boundary. This restriction permits an accounting for the relatively slow increase in nucleation kinetics observed with decreasing reaction temperature in the previous study of Fe-C alloys.

The purpose of the present investigation is to examine the influence of several representative substitutional alloying elements upon the nucleation kinetics of proeutectoid ferrite allotriomorphs at austenite grain boundaries in high purity Fe-C-X alloys, where X is successively Mn, Ni, Co, Si, and Mo, taking advantage of the experimental techniques and nucleus models developed in the previous investigation.[5] Although the introduction of a second solute increases the requirements for ancillary data needed to calculate nucleation kinetics, theoretical schemes are available through which the influence of X upon the volume free energy change attending nucleation and the energy of the austenite grain boundaries can be estimated. The alloying elements were chosen to show a variety of characteristics with respect to α-γ equilibria and interaction with carbon. They also are expected to vary in their tendency for segregation to austenite grain boundaries.

The Fe-C-Mo alloy is of special interest. It is well known that the TTT-curve for the beginning of transformation in this system usually exhibits a deep bay. The parabolic rate constant for the thickening kinetics of grain boundary allotriomorphs varies with temperature in a manner nearly a mirror image to that of the TTT-curve.[8] It is thus important to ascertain whether or not nucleation kinetics exhibit similar, or some other behavior in and near the bay region.

A TEM study of the Mn, Ni, and Si alloys used in this study indicates that carbide precipitation in the reaction time-temperature ranges of interest occurs only within ferrite and takes place after the formation of ferrite has begun.[9] A similar situation is likely to obtain in the Fe-C-Co alloy. Although M_2C precipitation in conjunction with ferrite takes place voluminously in the Fe-C-Mo alloy employed, these carbides also do not initiate transformation at the austenite grain boundaries.[10] Some prior formation of M_6C at grain boundaries was observed but was found to be of only minor significance[10,11] in the temperature region investigated.

II. EXPERIMENTAL PROCEDURES

Table I gives the compositions of the vacuum-melted, vacuum-cast alloys being used in this study and also certain characteristics of the alloying elements. The concentrations of carbon and alloying element are all approximately 0.5 and 3 at. pct, respectively, except in the Mo alloy where rapid constriction of the austenite region by Mo required the use of a lower concentration of Mo and a higher proportion of C.[10] The positive and negative signs of the Wagner interaction parameter in Table I correspond to repulsive and attractive interactions, respectively, between carbon and the substitutional solute, X, in austenite.

Bars of these alloys were homogenized for three days at 1300 °C. Square samples 6×10^{-3} m on edge and 1.5×10^{-4} m thick taken from the homogenized bars were austenitized for 30 minutes at 1300 °C in an argon atmosphere-protected, graphite-deoxidized bath of molten $BaCl_2$,[12] isothermally reacted in a graphite-covered lead bath and ice-brine quenched. They were then tempered for 15 minutes at approximately 300 °C in order to aid etching of the former austenite grain boundaries. The austenitizing time was chosen so that most of the boundaries become nearly perpendicular to the plane of polish established on the broad faces of the specimens. This geometry has been shown to be a prerequisite for applying the Schwartz-Saltykov method to the precipitates in the boundary plane, and also for facilitating discrimination between austenite grain face and edge nucleation.[5]

After heat treatment, specimens were mechanically polished and etched in two successive solutions: 50 ml saturated picric acid and 50 ml Teepol for grain boundary etching, and 7.8 gm oxalic acid, 108 ml H_2O, and 6 ml H_2O_2 for revealing the martensite matrix and the ferrite allotriomorphs at the grain boundaries.[5] After a grid 5×10^{-4} m square was developed on the plane of polish using a photo-sensitive lacquer,[13] the number of allotriomorphs per unit area was counted as a function of reaction time and temperature and converted to the actual number of allotriomorphs per unit area of unreacted austenite grain boundary. The details of these procedures have been previously described.[5]

III. RESULTS

In Figure 2, a scanning electron micrograph of an intergranularly fractured specimen of an Fe-0.5 at. pct C-

Table I. Chemical Compositions of Alloys and Characteristics of Substitutional Alloying Elements

Alloy	Wt Pct C	At. Pct C	Wt Pct X	At. Pct X	Wt Pct Mn	Wt Pct Si	Wt Pct P	Wt Pct S	α or γ Stabilizer	$\varepsilon_{c,\gamma}^{(2)}$* at 1000 °C
Fe-C-Mn	0.11	0.49	3.08	3.12	—	0.080	0.001	0.007	γ	−4.4
Fe-C-Ni	0.11	0.51	3.28	3.11	<0.002	0.001	0.001	0.004	γ	4.1
Fe-C-Co	0.12	0.54	3.16	2.97	—	—	—	—	α (weak)	2.3
Fe-C-Si	0.11	0.50	1.83	3.56	<0.002	—	0.002	0.007	α	9.9
Fe-C-Mo	0.18	0.84	4.25	2.48	<0.003	0.009	0.002	0.002	α	−8.5

*$\varepsilon_{c,\gamma}^{(2)}$ is the Wagner interaction parameter in austenite. It is defined by $\varepsilon_c^{(2)} = (\partial \ln \gamma_c)/(\partial x_2)_{x_2=0}$, where 2 denotes the alloying element X. γ_c is the activity coefficient of carbon in austenite.

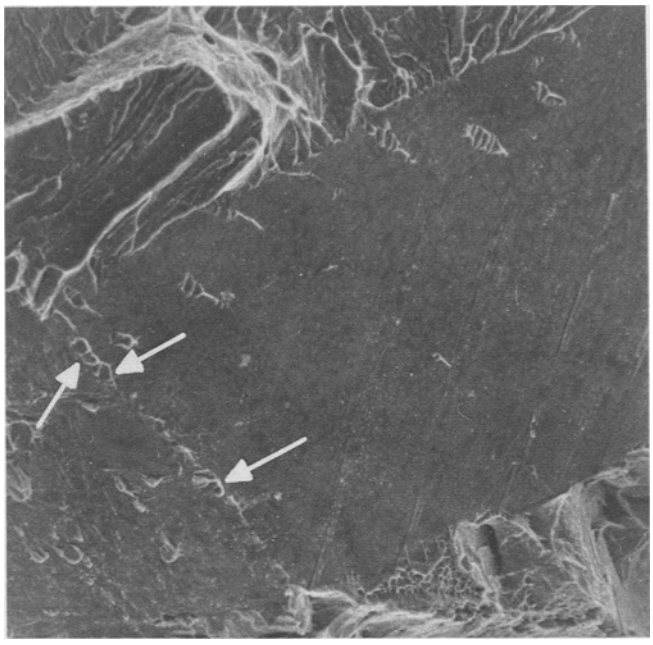

Fig. 2—SEM micrograph of ferrite allotriomorphs formed at austenite grain boundary face: an intergranular fracture surface of Fe-0.5 at. pct C-3 at. pct Ni, austenitized at 1300 °C for 30 min, isothermally reacted at 710 °C for 20 sec, and fractured at room temperature. Magnification 666 times.

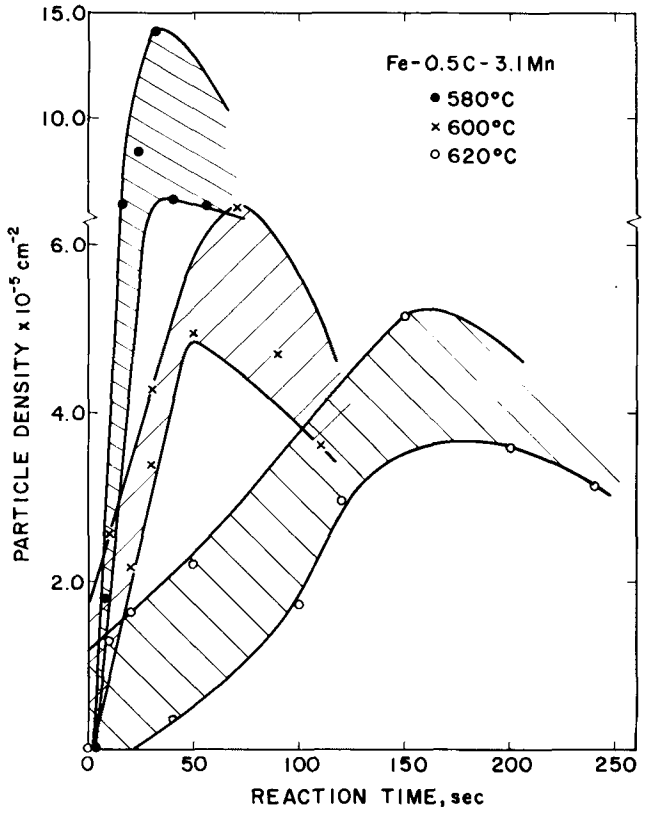

Fig. 3—Particle density *vs* reaction time plot for Fe-0.5 at. pct C-3 at. pct Mn alloy.

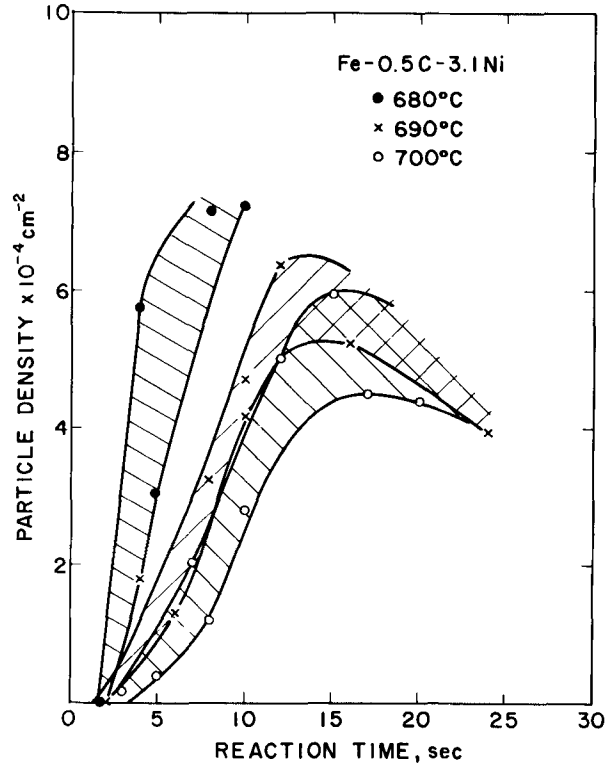

Fig. 4—Particle density *vs* reaction time plot for Fe-0.5 at. pct C-3 at. pct Ni alloy.

3 at. pct Ni alloy* provides a "face on" view of ferrite allotriomorphs along austenite grain faces.

*The other alloys containing 0.5 at. pct C did not fracture intragranularly.

Figures 3 through 7 show the plots of the observed number of face-nucleated ferrite particles per unit unreacted grain boundary area, also termed the particle density, as a function of the isothermal reaction time. The temperature range over which the measurements were made was the widest experimentally accessible in each alloy. This was 20 °C in the Ni and Co alloys and 40 °C in the Mn and Si alloys. In the Mo alloy, the much slower transformation kinetics permitted data collection over a range of approximately 300 °C, from the bay temperature to a temperature above the nose of the upper C-curve.

The decreasing numbers of allotriomorphs at grain faces observed at later reaction times in many of the plots in Figures 3 through 7 may be attributed to a combination of the impingement of adjacent face-nucleated allotriomorphs, the difficulty in revealing ferrite:ferrite boundaries with the etchants used, and the growth of face-nucleated allotriomorphs to the grain edges;* coarsening might also have been responsible for some part of the decrease, though only at late stages of reaction when overlapping of diffusion fields finally becomes significant.

*The particles in contact with junctions of three grain boundaries, *i.e.*, "triple points", were all regarded as edge-nucleated.

The conversion of the plots in Figures 3 through 7 to nucleation rates requires that the slope of the curves be plotted as a function of time. However, due to the scatter in the data, it was decided to calculate the slopes allowable in the scatterbands and take them as the probable range of J_s^*, the steady state nucleation rate per unit unreacted grain boundary area, neglecting the brief initial transient period. The J_s^* values thus determined are summarized in Table II. This table also includes the calculated and experimen-

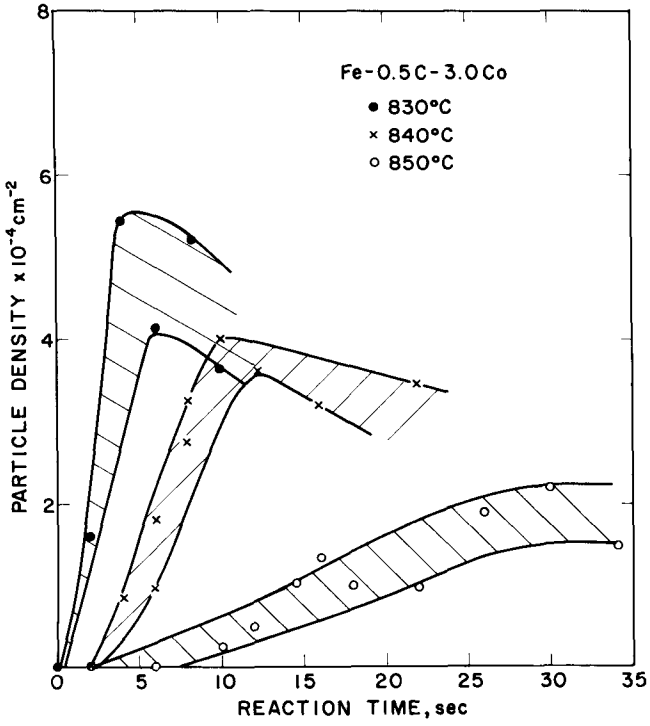

Fig. 5 — Particle density *vs* reaction time plot for Fe-0.5 at. pct C-3 at. pct Co alloy.

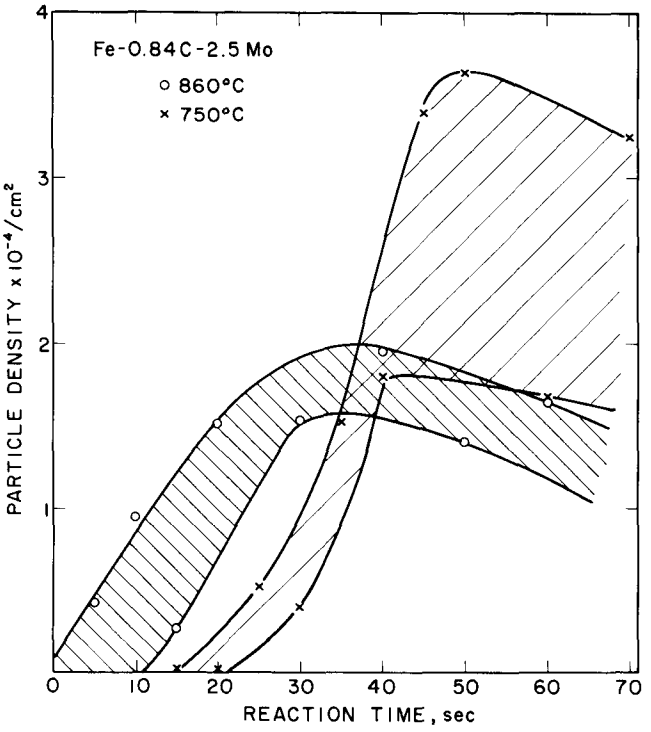

(*a*)

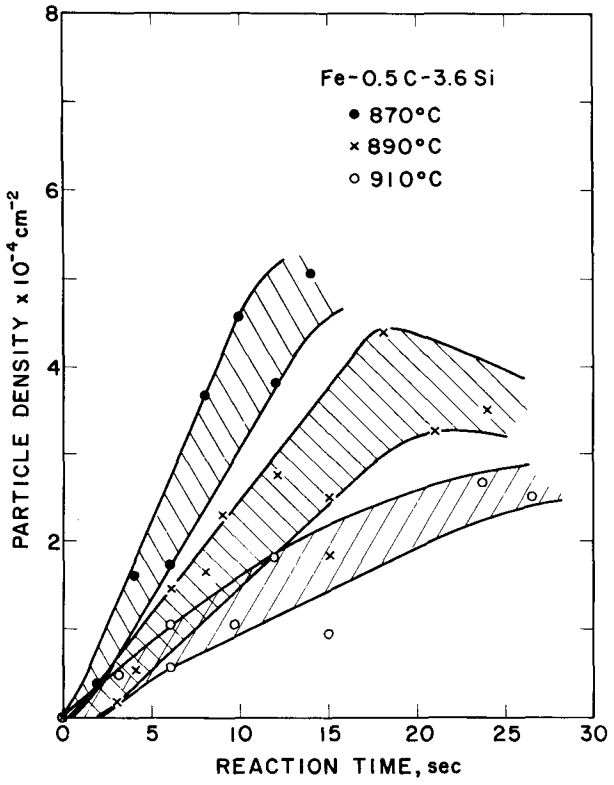

Fig. 6 — Particle density *vs* reaction time plot for Fe-0.5 at. pct C-3 at. pct Si alloy.

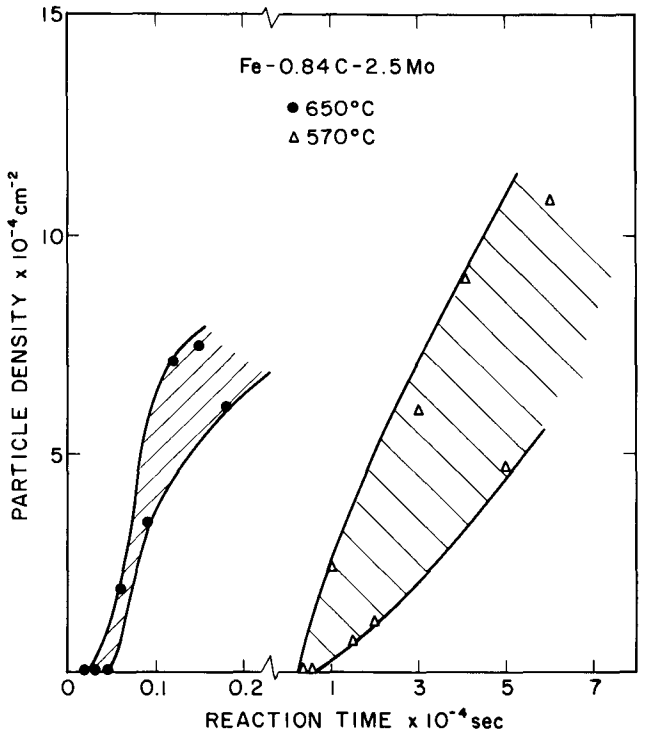

(*b*)

Fig. 7 — Particle density *vs* reaction time plot for Fe-0.5 at. pct C-3 at. pct Mo alloy: (*a*) for two higher temperatures and (*b*) for two lower temperatures.

tally determined $\gamma/(\alpha + \gamma)$ temperatures, the calculated no-X-partition temperature (paraequilibrium $\gamma/(\alpha + \gamma)$ boundary), and the volume free energy change at each reaction temperature. The calculation of each of these quantities is described in subsequent sections.

It is seen that both the reaction temperature and the amount of undercooling which give rise to similar J_s^* values vary widely with the alloying element.

Table II. Measured Nucleation Rates

Alloy	Temperature, °C: $\gamma/(\alpha+\gamma)$ Calc. / Exptl.	Temperature, °C: No-Partition Boundary	Temperature of Measurement, °C	J_s^*(cm$^{-2}\cdot$s^{-1})	ΔG_v(J·cm^{-3})†† Paraequilibrium	ΔG_v(J·cm^{-3})†† Orthoequilibrium
Fe-C-Mn	775 / 765	735	620	$(2.8 \pm 0.9) \times 10^3$	− 54.3	− 74.5
			600	$(8.3 \pm 1.5) \times 10^3$	− 67.8	− 88.8
			580	$(3.5 \pm 1.5) \times 10^4$	− 81.9	−103.9
Fe-C-Ni	785 / 775	770	700	$(5.1 \pm 1.4) \times 10^3$	− 19.2	− 28.6
			690	$(6.0 \pm 0.8) \times 10^3$	− 23.8	− 33.2
			680	$(1.6 \pm 0.7) \times 10^4$	− 30.3	− 38.2
Fe-C-Co	885 / —†	880	850	$(8.7 \pm 2.4) \times 10^2$	− 6.6	− 7.8
			840	$(4.6 \pm 0.8) \times 10^3$	− 9.3	− 10.6
			830	$(1.2 \pm 0.6) \times 10^4$	− 12.1	− 13.5
Fe-C-Si	1000 / 990	995	910	$(1.2 \pm 0.3) \times 10^3$	− 10.2	− 12.0
			890	$(2.2 \pm 0.6) \times 10^3$	− 14.3	− 16.5
			870	$(4.1 \pm 1.0) \times 10^3$	− 17.8	− 20.3
Fe-C-Mo	935 / —	930	860	$(6.7 \pm 1.5) \times 10^2$	− 6.9	− 7.7
			750	$(1.3 \pm 0.5) \times 10^3$	− 33.9	− 34.6
			650	$(7.0 \pm 1.2) \times 10^1$	− 87.8	− 88.7
			570	1.7 ± 0.7	−149.3	−150.8

†Not measured.
††ΔG_v is the volume free energy change attending ferrite nucleation.

IV. DISCUSSION

A. *The Effect of Growth Kinetics on Measured J_s^* Values*

It is reported that some solute elements are remarkably effective in decreasing the growth kinetics of ferrite allotriomorphs.[14] Therefore, it is necessary to estimate how much the growth kinetics affect measurement of the nucleation rate. In Table III, the time, t_G, for the ferrite particles to grow to 1 μm, the approximate resolution limit of the optical microscope, at a representative reaction temperature in each alloy is given on the basis of parabolic rate constant data published for these alloys.[6,14,15] Including even the Mo alloy, all t_G are less than ⅕ of the time at which the particle density reaches its maximum value. Nonetheless, the Schwartz-Saltykov method was applied to the virtual size distribution of allotriomorphs back-calculated from the observed size distribution on the plane of polish at time $t + t_G$ for a few sets of data. However, this procedure merely shifted the time scale without significantly altering the slope of particle density *vs* time plots, probably because the t_G values are so small relative to those of t.

Table III. Time for a Ferrite Allotriomorph to Grow to 1 μm, t_G

Alloy	Temperature, °C	t_G, Sec	Ref.
Fe-C-Mn	580	5.9	14
Fe-C-Ni	680	1.4	14
Fe-C-Co	820	0.03	15
Fe-C-Si†	910	1.2	15
Fe-C-Mo††	570	1.6×10^4	10

†Fe-0.5 at. pct C-2.7 at. pct Si alloy.
††No data at high temperatures.

B. *Analysis of the Nucleation Rate Data*

Classical nucleation theory expresses the time dependent nucleation rate, J_s^*, as:[16,17]

$$J^* = N\beta^* Z \exp\left(-\frac{\Delta G^*}{kT}\right) \exp\left(-\frac{\tau}{t}\right) \qquad [1]$$

where N is the density of viable atomic nucleation sites, β^* is the frequency factor, Z is the Zeldovich nonequilibrium factor, ΔG^* is the free energy of activation for formation of the critical nucleus, τ is the incubation time, t is the isothermal reaction time, and kT has its usual meaning. The time-independent portion of this equation is termed the steady state nucleation rate, J_s^*.

The pillbox model of Figure 1(a) will be used to analyze the results of the present investigation. Equation [1] thus becomes:[5]

$$J_s^* = N \cdot \frac{2DX^B V_\alpha \varepsilon^{1/2}}{a^4(3kT)^{1/2}} \exp\left[\frac{4\pi(\sigma_{\alpha\gamma}^e)^2 \varepsilon}{\phi^2 kT}\right] \qquad [2]$$

$$\phi = \Delta G_v + W \qquad [3\text{-A}]$$

$$\varepsilon = \sigma_{\alpha\gamma}^c + \sigma_{\alpha\gamma}^{cb} - \sigma_{\gamma\gamma} \qquad [3\text{-B}]$$

where D is the appropriate diffusivity, X^B is the atom fraction of solute in the parent austenite,* V_α is the molar volume of ferrite (= 7.09 cm^3/mole), a is approximately the average lattice parameter of α and γ, ΔG_v is the volume free energy charge, and W is the strain energy associated with the nucleus. $\sigma_{\alpha\gamma}^e$, $\sigma_{\alpha\gamma}^c$, $\sigma_{\alpha\gamma}^{cb}$, and $\sigma_{\gamma\gamma}$ are the energies of the interfaces indicated in Figure 1. The radius, r^*, and height, h^*, of the critical nucleus are:

*When the austenite is enriched in a solute, X^B is replaced by $1 - X^B$.[18]

$$r^* = -\frac{2\sigma^e_{\alpha\gamma}}{\phi} \qquad [4\text{-A}]$$

$$h^* = -\frac{2\varepsilon}{\sigma} \qquad [4\text{-B}]$$

C. *Calculation of Volume Free Energy Change Associated with Nucleation*

Correct evaluation of the volume free energy change is very important for the interpretation of nucleation kinetics data. Although ΔG_v is customarily evaluated at either the equilibrium composition or the composition yielding the maximum $|\Delta G_v|$, the critical nucleus composition is different from both of them due to the presence of capillarity.[18] However, calculations of the critical nucleus composition of ferrite incorporating the capillarity effect for the Mn alloy used in this investigation have shown that the error involved when the equilibrium composition is used to evaluate ΔF_v is negligible because of the small carbon concentration in ferrite, the relatively small difference in the partial molar volumes of Fe and C,[19] and the relatively high undercoolings at which the present measurements were conducted.[20]

Two solution models are employed to evaluate ΔG_v. One is the widely used Hillert-Staffanson (HS) regular solution model.[21] The other is the Central Atoms Model (CAM), the product of an advanced statistical thermodynamic analysis.[22,23,24] In a current paper, the $\alpha + \gamma$ phase boundaries and ΔG_v calculated from these two models are numerically compared for the proeutectoid ferrite reaction in Fe-C-X alloys having compositions the same as or similar to those used in this investigation.[25] The ancillary parameter data needed to use the Hillert-Staffanson model were taken from the compilation by Uhrenius[26] while those needed for the Central Atoms Model were largely drawn from analyses and summaries by Kaufman and Nesor[27] and Kirkaldy *et al.*[28] The two analyses yielded similar results, and in the case of phase boundary calculations compared well with experimental data.[25] The advantages which the Central Atoms Model may offer in respect of calculations for quaternary and higher order systems are presently being explored.[29]

Phase boundaries and ΔG_v were calculated on both the orthoequilibrium and paraequilibrium models of alloying element partition between austenite and ferrite. It is noted that all the nucleation rate measurements were conducted below the paraequilibrium $\gamma/(\alpha + \gamma)$ boundary (Table II). In the orthoequilibrium case, both phases achieve their full equilibrium compositions throughout; these compositions are obtained by solving three simultaneous equations:

$$\mu_{i,\alpha} = \mu_{i,\gamma} \quad \text{for } i = 1, 2, \text{ and C} \qquad [5]$$

In this set of equations, iron, X, and carbon are denoted as 1, 2, and C, respectively. The μ_i's are the chemical potentials of the i'th species at equilibrium in ferrite or austenite. In the paraequilibrium case, partition of carbon takes place between austenite and ferrite, but the original bulk concentration of X is inherited by the ferrite. Paraequilibrium compositions are derived from the solutions of two simultaneous equations:[30,31]

$$\mu_{c,\alpha} = \mu_{c,\gamma} \qquad [6\text{-A}]$$

$$Y_{1,\alpha}\mu_{1,\alpha} + Y_{2,\alpha}\mu_{2,\alpha} = X_{1,\gamma}\mu_{1,\gamma} + X_{2,\gamma}\mu_{2,\gamma} \qquad [6\text{-B}]$$

under the condition:

$$Y_{2,\alpha} = Y_{2,\gamma} = (X_2/X_1)^\beta \qquad [7]$$

Here, Y_i is the ratio of the number of the i'th species atoms to the total number of sites in the sublattice to which these atoms belong. They are written in terms of X_i as:

$$Y_1 = \frac{X_1}{1 - X_c}, \qquad Y_2 = \frac{X_2}{1 - X_c}, \qquad Y_c = \frac{X_c}{r(1 - X_c)} \qquad [8]$$

where X_1, X_2, and X_c are the atom fractions of Fe, X, and C, respectively, and r is the ratio of the number of interstitial sites to that of substitutional sites (3 for ferrite and 1 for austenite). In both types of equilibrium, ΔG_v is calculated from the equation:

$$\Delta G_v = \frac{1}{V_\alpha}\{\boldsymbol{\mu}_\gamma(\mathbf{X}_\gamma^{\gamma\alpha}) - \boldsymbol{\mu}_\gamma(\mathbf{X}_\gamma)\} \cdot \mathbf{X}_\alpha^{\alpha\gamma} \qquad [9]$$

where $\boldsymbol{\mu} = (\mu_1, \mu_2, \mu_c)$ and $\mathbf{X} = (X_1, X_2, X_c)$ are vectors. $\mathbf{X}_\gamma^{\gamma\alpha}$ and $\mathbf{X}_\alpha^{\alpha\gamma}$ denote the equilibrium compositions in austenite and ferrite, respectively.

Figure 8 shows the ortho- and paraequilibrium $\gamma/(\alpha + \gamma)$ phase boundaries calculated for each alloy used from the HS model except for the Co alloy.* Figure 9 is an

*The data on the parameters for the Fe-C-Co system are not available in the compilation of Reference 26. Accordingly, this calculation was conducted only through the CAM.

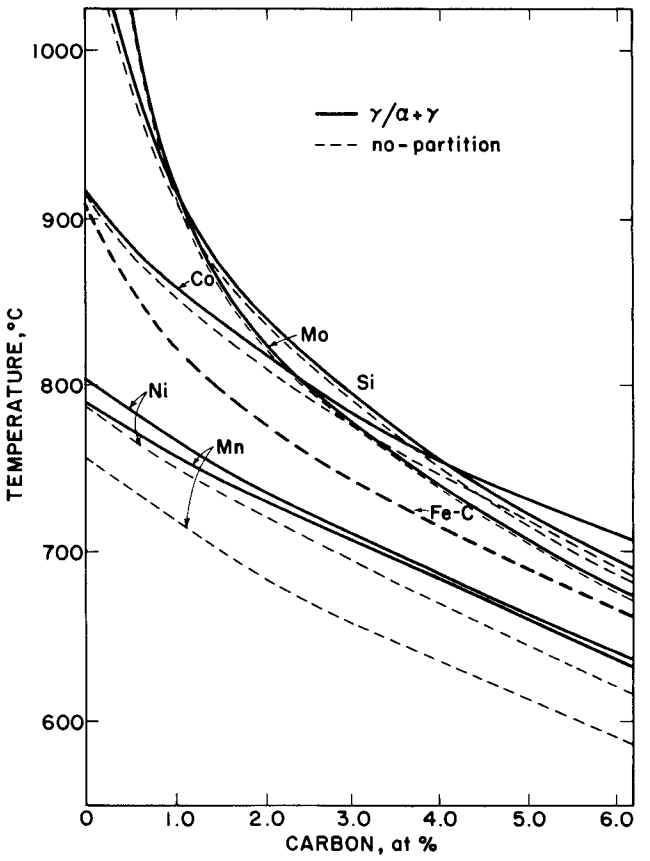

Fig. 8—Orthoequilibrium $\gamma/(\alpha + \gamma)$ and no-partition boundaries in the alloys studied. The curve for an Fe-C alloy is included for reference purposes.

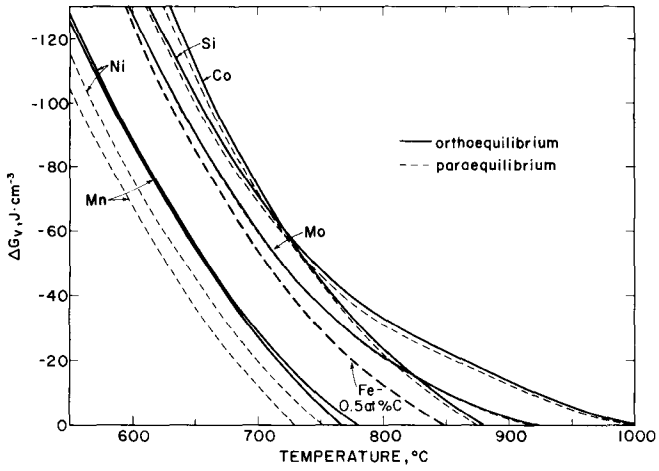

Fig. 9—Volume free energy change of proeutectoid ferrite reaction in alloys studied.

equivalent presentation for ΔG_v. The curves for an Fe-0.5 at. pct C alloy are included for reference purposes.

V. ANALYSIS OF NUCLEATION RATE MEASUREMENTS

Assuming that, in Eq. [2], N and $\theta \equiv (\sigma^e_{\alpha\gamma})^2\varepsilon$ are constants in the temperature ranges in which the measurements were made, the ranges of their values which give the ranges of measured J_s^* values were determined. The results are recorded in the first and the second columns of Tables IV-a through c. The assumption that N and θ are constant is not unreasonable for the Mn, Ni, Si, and Co alloys because the temperature ranges in which kinetics could be measured are only 20 to 40 °C. In the Fe-C-Mo alloy the temperature range available was about an order of magnitude larger. Accordingly, the J_s^* at the two highest temperatures were used, though the 110 °C temperature difference between them is still much wider than for the other alloys.

In respect of the diffusivity term in Eq. [2], three different options were examined. If paraequilibrium ferrite nuclei are formed (Case I), the volume diffusivity of carbon in austenite is appropriate. The relationship derived by Kaufman, Radcliffe, and Cohen[32] for this diffusivity as a function of both temperature and carbon concentration was utilized. If the ferrite nuclei are of orthoequilibrium composition (Case II), mass transport of X will presumably be rate-controlling. This can be accomplished by either volume diffusion through austenite (Case II-1) or by diffusion along austenite grain boundaries and austenite:ferrite boundaries (Case II-2).[33] The correlations developed by Fridberg *et al.*[34] for volume and boundary diffusion in substitutional Fe-base alloys were used in these situations.*

*It should be noted that on these correlations the boundary diffusion of X is only slightly more rapid than the volume diffusion of carbon in austenite.

The value of ε was calculated from the relationship of Eq. [4-B] assuming a pillbox nucleus of biatomic height at the lowest temperature of measurement. Subsequently, $\sigma^e_{\alpha\gamma}$ was calculated from the θ values and r^* from Eq. [4-A].

Compared to the $\sigma^e_{\alpha\gamma}$ of 18 erg/cm^2 in an Fe-0.6 at. pct C alloy determined with a similar procedure,[5] the values for ternary alloys are mostly larger. As in the previous study,[5] it is reasonable to assume that the rim of a thin pillbox nucleus is fully coherent. At the present time we are unable

Table IV. Calculated Values of Viable Nucleation Site Density, Interfacial Energies, and Critical Nucleus Size

a. Paraequilibrium: Volume Diffusion of Carbon in Austenite

Alloying Element	N cm^{-2}	$\theta\left(\frac{\text{ergs}}{\text{cm}^2}\right)^3$	$\varepsilon\left(\frac{\text{ergs}}{\text{cm}^2}\right)$	$\sigma^e_{\alpha\gamma}\left(\frac{\text{ergs}}{\text{cm}^2}\right)$	r^* at the Lowest Temperature (Number of Atomic Planes)
Mn	$10^{1\text{ to }2}$	$(1.8 \pm 0.4) \times 10^4$	5.5	51 to 64	9.4 to 12
Ni	$10^{-1\text{ to }0}$	$(4.7 \pm 2.6) \times 10^2$	1.9	11 to 20	5.7 to 10
Co	$10^{-1\text{ to }0}$	$(2.2 \pm 0.5) \times 10^2$	0.7	16 to 20	24 to 30
Si	$10^{-2\text{ to }-1}$	$(7.0 \pm 2.5) \times 10^1$	1.0	7.0 to 9.7	6.9 to 9.5
Mo	$10^{-2\text{ to }-1}$	$(1.8 \pm 0.6) \times 10^2$	3.4	17 to 25	5.9 to 8.4

b. Orthoequilibrium: Volume Diffusion of Alloying Element in Austenite

Alloying Element	N cm^{-2}	$\theta\left(\frac{\text{ergs}}{\text{cm}^2}\right)^3$	$\varepsilon\left(\frac{\text{ergs}}{\text{cm}^2}\right)$	$\sigma^e_{\alpha\gamma}\left(\frac{\text{ergs}}{\text{cm}^2}\right)$	r^* at the Lowest Temperature (Number of Atomic Planes)
Mn	$10^{8\text{ to }9}$	$(5.2 \pm 1.0) \times 10^4$	7.5	75 to 91	10 to 12
Ni	$10^{6\text{ to }7}$	$(3.5 \pm 1.5) \times 10^3$	2.9	26 to 42	9.1 to 15
Co	$10^{4\text{ to }5}$	$(3.5 \pm 0.7) \times 10^2$	0.8	19 to 23	24 to 30
Si	$10^{4\text{ to }5}$	$(1.0 \pm 0.2) \times 10^3$	1.2	26 to 31	22 to 26
Mo	$10^{5\text{ to }6}$	$(3.0 \pm 0.6) \times 10^2$	3.5	8.3 to 10	24 to 29

c. Orthoequilibrium: Boundary Diffusion of Alloying Element

Alloying Element	N cm^{-2}	$\theta\left(\frac{\text{ergs}}{\text{cm}^2}\right)^3$	$\varepsilon\left(\frac{\text{ergs}}{\text{cm}^2}\right)$	$\sigma^e_{\alpha\gamma}\left(\frac{\text{ergs}}{\text{cm}^2}\right)$	r^* at the Lowest Temperature (Number of Atomic Planes)
Mn	$10^{1\text{ to }2}$	$(4.1 \pm 1.0) \times 10^4$	7.5	64 to 83	8.6 to 11
Ni	$10^{0\text{ to }1}$	$(2.8 \pm 1.5) \times 10^3$	2.9	21 to 39	7.4 to 14
Co	$10^{-1\text{ to }0}$	$(3.3 \pm 0.8) \times 10^2$	0.8	18 to 23	23 to 29
Si	$10^{-2\text{ to }-1}$	$(8.5 \pm 3.0) \times 10^2$	1.2	21 to 31	18 to 26
Mo	$10^{-2\text{ to }-1}$	$(1.8 \pm 0.5) \times 10^2$	3.5	6 to 8	17 to 23

to calculate the temperature dependence of the $\alpha:\gamma$ interfacial energy with sufficient accuracy. From the work by Lee and Aaronson,[35] however, for the case of coherent fcc:fcc interfaces the temperature dependence of the interfacial energy can be deduced as $d\sigma/dT = -(0.2 \text{ to } 0.3)$ ergs/deg for $T/T_c \gtrsim 0.35$ where T_c is the critical temperature of the regular solution miscibility gap. This dependence seems to give a reasonable explanation for the relatively high $\sigma^e_{\alpha\gamma}$ values in the Ni and Mn alloys in which measurements were made at lower temperatures than in the Fe-0.6 at. pct C alloy (800 °C).

Of the three options, paraequilibrium gives somewhat too low $\sigma^e_{\sigma\gamma}$ values. Since the procedures utilized yield the largest possible value in each alloy, these results tend to favor the orthoequilibrium mode of ferrite nucleation. Whereas Case II-1, *i.e.*, orthoequilibrium with volume diffusion of X, gives reasonable values of both interfacial energies and N, Case II-2, orthoequilibrium with mass transport *via* boundary diffusion yields appropriate interfacial energies but values of N orders of magnitude below the experimentally observed number densities of grain boundary allotriomorphs at late reaction times. Nonetheless, we still consider that these results favor Case II-2. The primary reason for this choice simply is that in the Fe-C alloys reasonable interfacial energies but too low N values were also obtained.[5] The nonphysical results secured with respect to N were ascribed to differences between the pillbox model and the actual shape of the critical nuclei.[5]* Similar results have been found for the bcc$\beta \rightarrow$ hcpα massive transformation in Ti-Ag and Ti-Au alloys[36] and more recently for the proeutectoid α reaction in Ti-Co and Ti-Cr alloys.[37] Secondly, it is plausible to expect that the nucleus evolves to the critical size most readily when X atoms can diffuse along paths where their diffusivity is comparable to that of carbon in bulk austenite. Hence, we tentatively conclude that ferrite nuclei in Fe-C-X alloys in the temperature-composition regions investigated are of orthoequilibrium composition, with X transport during nucleation taking place by grain and interphase boundary diffusion.

*It must noted, however, that with all other quantities unchanged $\sigma^e_{\alpha\gamma}$ needs to be only 1.5 to 5× larger than the values given to make up the differences of 4 to 5 orders of magnitude between the calculated and experimentally observed N's.

Studies of both X partition[38] and growth kinetics of ferrite[14,15] in several Fe-C-X alloys have led to the conclusion that the allotriomorphs formed in the temperature ranges utilized in the present investigation are of paraequilibrium composition. This can be interpreted as follows. As particles grow, progressively more X atoms are necessary to maintain full equilibrium. The situation is soon reached in which X transport along the grain boundary is no longer sufficient to maintain the rapid increase in the particle volume, particularly when the growth rate is controlled by carbon diffusion.

Incorporation of volume strain energy can be attempted, at the present time, only by assuming that the pillbox nuclei are discs wholly imbedded within the matrix.[39] This increases $\sigma^e_{\alpha\gamma}$ by 20 to 30 pct in the alloys in which measurements were made at relatively low undercoolings. At larger undercoolings, the strain energy effect becomes less important. Hence the qualitative nature of the conclusions is not altered.

VI. INFLUENCE OF ALLOYING ELEMENT SEGREGATION UPON AUSTENITE GRAIN BOUNDARY ENERGY

As indicated by Eqs. [2] and [3-B], the energy of austenite grain boundaries, $\sigma_{\gamma\gamma}$, may play a major role in determining the nucleation kinetics of ferrite at these boundaries. Alloying element segregation to austenite grain boundaries has the potential for significantly reducing the energy, and thus the catalytic potency of such boundaries. Segregation to austenite:ferrite boundaries will have the reverse effect. However, the absence of experimental information with which to guide a treatment of the latter problem confines the considerations of this section to examination of segregation effects upon the energy of austenite grain boundaries.

A number of models is available with which to compute the decrease in grain boundary energy accompanying solute segregation.[40–44] Among them, the theory proposed by Guttmann and McLean[44] appears particularly useful in the present context as it incorporates the effect of interactive segregation between different species of solute atoms. A substantial amount of data on temper embrittlement can be readily explained by means of this theory.[44,45] The variant of the theory which assumes two kinds of solute atoms, *e.g.*, substitutional and interstitial, occupying different sublattices and thus segregating without "site competition", appears to be most appropriate for Fe-C-X alloys. The equations for segregation of carbon and substitutional alloying element to austenite grain boundaries appropriate to this model are:

$$\frac{Y^\phi_C}{(1 - Y^\phi_C)^{1+\Omega}(Y^\phi_1)^\Omega} = \frac{Y^B_C}{(1 - Y^B_C)^{1+\Omega}(Y^B_1)^\Omega} \exp\left(\frac{\Delta G_C}{RT}\right) \quad [10\text{-A}]$$

$$\frac{Y^\phi_2}{1 - Y^\phi_2} = \frac{Y^B_2}{1 - Y^B_2} \exp\left(\frac{\Delta G_2}{RT}\right) \quad [10\text{-B}]$$

$$\begin{aligned}\Delta G_C = \Delta G^\circ_C &- 2\beta_{CV}(Y^\phi_C - Y^B_C) + \beta_{2C}(Y^\phi_2 - Y^B_2) \\ &+ \Omega[-\beta_{12}\{(Y^\phi_2)^2 - (Y^B_2)^2\} \\ &\quad - \beta_{CV}\{(Y^\phi_C)^2 - (Y^B_C)^2\} \\ &\quad + \beta_{2C}(Y^\phi_2 Y^\phi_C - Y^B_2 Y^B_C)]\end{aligned} \quad [11\text{-A}]$$

$$\Delta G_2 = \Delta G^\circ_2 - 2\beta_{12}(Y^\phi_2 - Y^B_2) + \beta_{2C}(Y^\phi_C - Y^B_C) \quad [11\text{-B}]$$

where β_{CV}, β_{2C}, and β_{12} are the HS regular solution constants whose values were taken from the compilation of Uhrenius.[26] ΔG°_C and ΔG°_2 are the (average) binding free energy of carbon and of alloying element to the austenite grain boundaries in infinitely dilute solutions. Also, $\Omega \equiv \overline{A}_c/\overline{A}_1$ where $\overline{A}_c$ and $\overline{A}_1$ are the partial molar areas of C and of Fe, respectively. The partial molar area of substitutional solute is assumed equal to that of Fe. ϕ and B denote the interfacial and bulk phases, respectively. The theory assumes that the regular solution constants are the same in both phases. When Y^B_C is small, the energy of austenite grain boundaries with segregated solute atoms, $\sigma_{\gamma\gamma}$, is given by:

$$\begin{aligned}\sigma_{\gamma\gamma} = \sigma_1 \cdot \overline{A}_1 &+ RT \ln \frac{Y^\phi_1}{Y^B_1} + RT \ln(1 - Y^\phi_C) \\ &- \beta_{12}[\{(Y^\phi_2)^2 - Y^B_2)^2\} - \beta_{CV}(Y^\phi_C)^2 \\ &+ \beta_{2C}(Y^\phi_C Y^\phi_2 - Y^B_C Y^B_2)]\end{aligned} \quad [12]$$

where σ_1 is the energy of austenite grain boundaries in pure Fe. A Scanning Auger Microprobe (SAM) analysis was made of the boundary fracture surface in Fe-C-X alloys with similar alloying element concentrations but with 0.4 wt pct instead of 0.1 wt pct C.* X_2^ϕ determined by peak height ratio in the Auger spectrum was substituted into Eqs. [10] and [11] to calculate ΔG_2°.

*The alloys with 0.4 wt pct C fractured along the former austenite grain boundaries after quenching to martensite. The 0.1 wt pct C alloys, other than the one containing Ni, studied in the present investigation fractured by intragranular cleavage.

Table V summarizes the data needed to calculate the decrease in austenite grain boundary energy and its temperature dependence. ΔG_C° is estimated as 10 kJ/mole from the recent work of Bradley *et al.*[47]

Figures 10 and 11 show the calculated temperature dependence of boundary monolayer concentrations of carbon and alloying element and the decrease in austenite grain boundary energy, $\Delta\sigma_{\gamma\gamma} = \sigma - \sigma_1$, in the alloys studied in this investigation.* Of all the alloying elements studied, Mo has the largest tendency to segregate to the austenite grain boundaries and thereby decreases $\sigma_{\gamma\gamma}$ most effectively below 1000 °C; this tendency is strengthened by the co-segregation of carbon (Figure 10). Among the other alloying elements, the decreasing order of capability for reducing the grain boundary energy appears to be Si, Mn, Co, and Ni.

*In the calculation of $\Delta\sigma_{\gamma\gamma}$, A is taken to be 3.3×10^8 cm^2/mole.[46]

Since the ΔG_C° is rather small, the influence of carbon upon Y_2^ϕ and $\Delta\sigma_{\gamma\gamma}$ is generally not very significant except in the Mo alloys.

When the diffusivity of X in austenite is low, it is very likely that nucleation occurs before the system attains equilibrium segregation. The time to reach halfway to equilibrium segregation can be estimated from an equation derived by D. McLean:[48]

$$t_{1/2} = \frac{9q^2\delta^2}{64D_2^V} \qquad [13]$$

where δ is the grain boundary thickness, D_2^V is the volume diffusion coefficient of X in austenite, and q is the enrichment factor at equilibrium, the values of which were taken from Figure 10(b). In Table VI, $t_{1/2}$ is compared to the time range of the nucleation rate measurements, t_M. The value of $t_{1/2}$ does not vary significantly in the temperature range in which measurements were made for alloys other than the Mo alloy. For this alloy the values at two temperatures are shown. It is seen that in the Ni, Co, and Si alloys, $t_{1/2}$ is very small compared to t_M. It is appropriate, then, to assume that equilibrium segregation is achieved before nucleation takes place in these alloys. However, in the Mn and Mo alloys the system is unlikely to be at equilibrium during nucleation. Thus the problem arises of estimating the energy of a

Table V. SAM Data on Segregation of X to Austenite Grain Boundaries

Alloying Element	Temperature of Measurement, °C	Enrichment Factor, q, in 0.4 Wt Pct Alloys	$\Delta G_2^{\circ\dagger}$ kJ/mole
Mn	1125	2.2	8
Ni	900 to 1100	1.0	<5
Co	1050 to 1100	1.0	<8
Si	1050	2.4	20
Mo	1200 to 1300	5.9	18

†Error caused by uncertainty in determining the boundary concentration does not exceed approximately 25 pct.

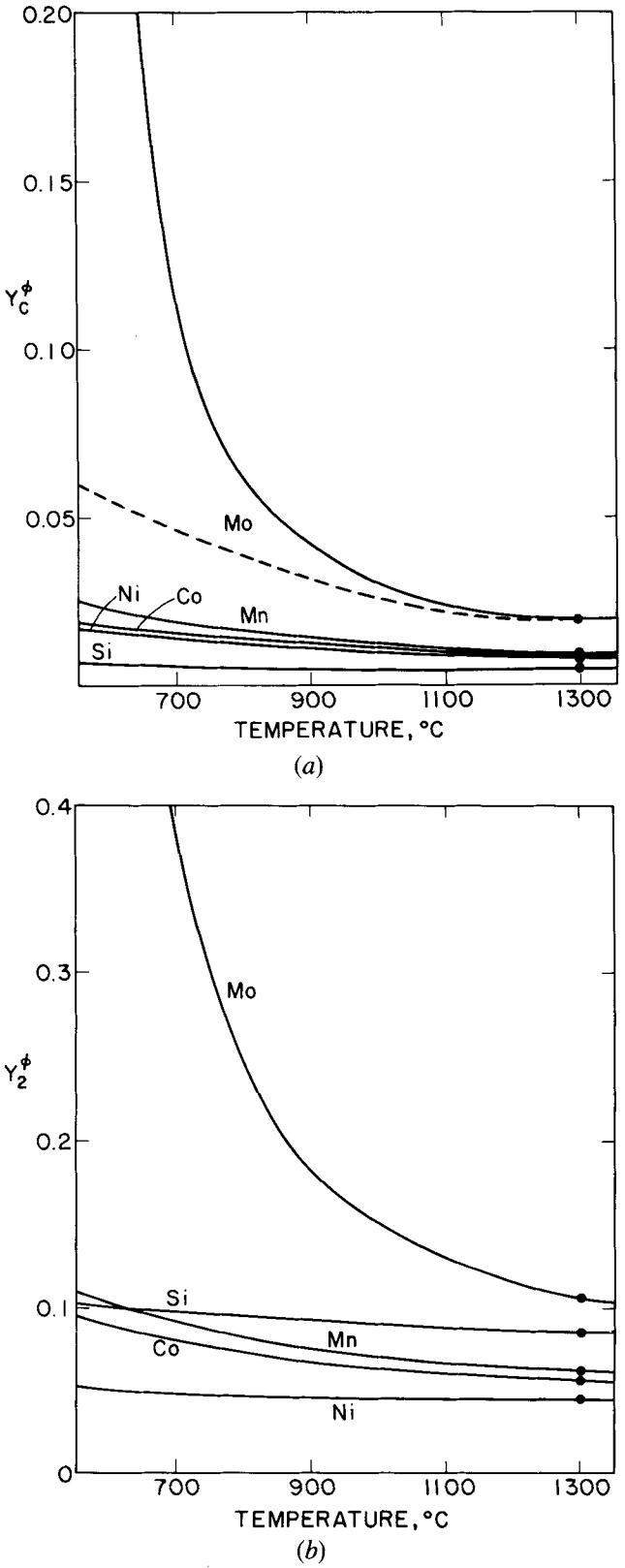

Fig. 10—Calculated grain boundary concentration of: (*a*) carbon X_c^ϕ, and (*b*) alloying elements X_2^ϕ, as functions of temperature in alloys studied. The dashed curve shows the concentrations in "as-quenched" boundaries (see text), while the solid curves show those at equilibrium.

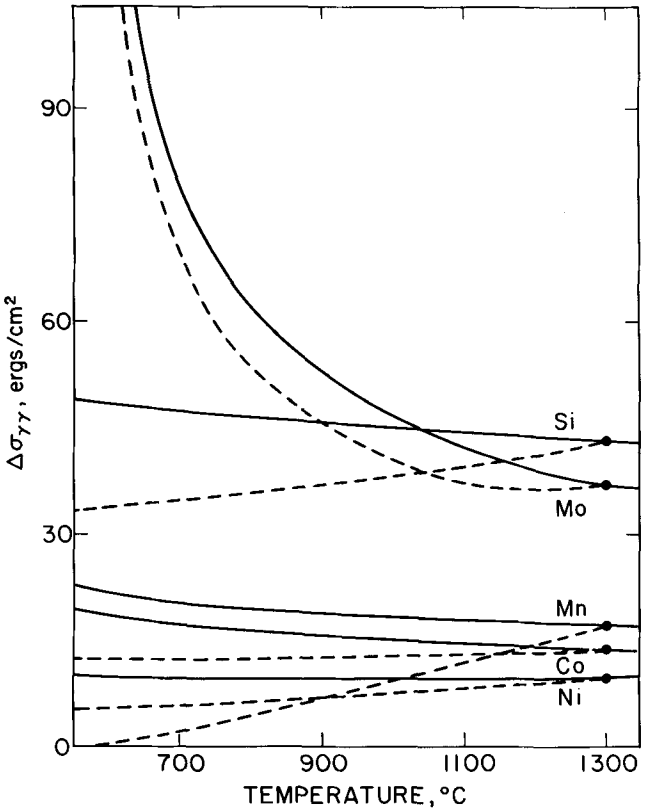

Fig. 11—Calculated austenite grain boundary energy decrease, $-\Delta\sigma_{\gamma\gamma}$, due to solute segregation as a function of temperature in the alloys studied. The dashed curves show the reduction in the energy of "as-quenched" boundaries while the solid curves show those at equilibrium.

boundary which is not in compositional equilibrium with its surroundings. The extremum situation is analyzed in which the boundary inherits the X concentration which it acquired at the austenitizing temperature but equilibrium is attained with respect to carbon at the reaction temperature.[46] The formalism used is similar to that for paraequilibrium, but Y_2 is not the same for the boundary and the bulk phases (see Eq. [7]). The segregation equation for carbon is the same as Eq. [10-A], but Y_2^ϕ is kept constant at the value for the austenitizing temperature, T_γ, while Y_2^B is also constant. For $Y_C^{B(\prime)}$, only the result appropriate to the Mo alloy is shown in Figure 10(b). In the other alloys, it is not much different from that of orthoequilibrium. Rewriting Eq. [6-B] in terms of Y_2^B and Y_2^ϕ,

$$Y_1^\phi\mu_1^\phi + Y_2^\phi\mu_2^\phi = Y_1^B\mu_1^B + Y_2^B\mu_2^B \qquad [14]$$

Eq. [14] is used to obtain the following $\Delta\sigma_{\gamma\gamma}$ relationship:

$$\begin{aligned}\Delta\sigma_{\gamma\gamma}\cdot A = &-Y_2^\phi\cdot\Delta G_2^\circ + (Y_2^\phi - Y_2^B)(\mu_2^{\circ B} - \mu_1^{\circ B})\\ &+ RT\{Y_1^\phi \ln Y_1^\phi + Y_2^\phi \ln Y_2^\phi + \ln(1 - Y_C^\phi)\\ &- \beta_{12}Y_1^\phi Y_2^\phi - \beta_{CV}(Y_C^\phi)^2\}\\ &- RT\{Y_1^B \ln Y_1^B + Y_2^B \ln Y_2^B - \beta_{12}Y_1^B Y_2^B\}\end{aligned} \qquad [15]$$

The calculated values of $\Delta\sigma_{\gamma\gamma}$ for T_γ = 1300 °C are summarized in Figure 11. These are considered to correspond to the state of the boundary immediately after quenching to the reaction temperature, and thus to the lower limit of $\Delta\sigma_{\gamma\gamma}$ at each temperature during nucleation. With increasing reaction time, $\Delta\sigma_{\gamma\gamma}$ becomes more negative, approaching the equilibrium values given in these figures. The $\Delta\sigma_{\gamma\gamma}$ values at the temperatures of measurement both for the equilibrium and the as-quenched situations are included in Table IV.

From Eq. [3-B] it is seen that a reduction in the austenite grain boundary energy increases ε. Before comparing the $\Delta\sigma_{\gamma\gamma}$ with the ε values in Table IV-c, it is noted that in an Fe-0.6 at. pct C alloy, ε = 0.5 ergs/cm².[5] Table IV-c shows that in all of the ternary alloys studied, ε is increased, and $\Delta\sigma_{\gamma\gamma}$ is always greater than ε.* This latter result indicates that the alloying elements also reduce the energies of nucleus:matrix boundaries but do so less extensively than those of austenite grain boundaries. Segregation of X to $\alpha:\gamma$ boundaries and reduction in the energy of such boundaries to lesser degrees than is accomplished at austenite grain boundaries can explain this finding. These lower levels of segregation are consistent with the high levels of coherency expected at nucleus:matrix boundaries (Figure 10) and perhaps also with the observation that the energy of at least disordered interphase boundaries is less than that of disordered grain boundaries in many alloy systems, including Fe-C.[50]

*In the Mn alloy, an apparent exception to this statement, the actual $\Delta\sigma_{\gamma\gamma}$ may also be larger than ε because $t_{1/2}$ is not much larger than t_M in this alloy and quenched-in vacancies usually expedite achievement of equilibrium.

However, arrangement of the elements in the order of their ability to increase ε does not yield the sequence of increasing $\Delta\sigma_{\gamma\gamma}$ calculated using the SAM data. A possible reason for the apparent lack of correlation between the ε and the $\Delta\sigma_{\gamma\gamma}$ changes is segregation of other minor impurities such as P and S, *etc.* to the austenite grain boundaries. The data on these elements reported by Hondros,[42] however, indicate that P and S of the same impurity levels as in the present alloys (see Table I) reduce the grain boundary energy only by 1 to 2 ergs/cm². Also, there were no indi-

Table VI. Comparison of Time of Measurement, t_M, Time to Reach Halfway to Equilibrium, $t_{1/2}$, at Lowest Temperature of Measurement,† and Reduction in Austenite Grain Boundary Energy, $\Delta\sigma_{\gamma\gamma}$

Alloying Element	t_M Sec.	$t_{1/2}$ Sec.	$\Delta\sigma_{\gamma\gamma}$ ergs/cm²	
			As-Quenched	Equilibrium
Mn	250	3.0×10^2	1	22
Ni	<25	3.7×10^0	<5	<10
Co	<34	2.1×10^{-3}	<13	<15
Si	<27	3.3×10^{-3}	34	44
Mo†	<70	6.7×10 (750 °C)	60	68
	$<6 \times 10^4$	6.2×10^5 (570 °C)	167	175

†Two temperatures for the Mo alloy.

cations in the Auger spectra that certain alloying elements, *e.g.*, Mn and Ni, *etc.*, induce exceptional cosegregation of these impurities to the austenite grain boundaries. Hence, it seems most likely at the present time that the ability of alloying elements to introduce $\Delta\sigma_{\gamma\alpha}$ is not exactly parallel to their capability for producing $\Delta\sigma_{\gamma\gamma}$.

VII. THE OVERALL EFFECT OF ALLOYING ELEMENTS ON J_s^*

In Figure 12, J_s^* is calculated over an extended range of temperatures for each alloy studied, assuming the constant N and θ values determined in the previous section. The equivalently calculated curve for an Fe-0.6 at. pct C alloy[5] is reproduced in this figure for comparative purposes. Although the values determined for Case II-2 are used, similar curves are obtained for the other two cases except for minor differences far from the temperature range in which the experimental measurements were made. The curve for the Mo alloy does not fit the experimental data at low temperatures. This is reasonable because the parameters were determined from the J_s^* data at two high temperatures in this alloy. This procedure implies that the amount of Mo segregation does not increase above the small value of the higher temperatures in the calculation; thus, at least the sign of the difference between the calculated and measured J_s^* curves at lower temperatures can be explained. As seen in Figure 12, Mn reduces J_s^* of ferrite most effectively and Ni does so next primarily because this is the order of the largest decrease in the $\gamma/(\alpha + \gamma)$ temperature and in $|\Delta G_v|$ effected per at. pct X for the alloying elements studied. Co, Mo, and Si increase J_s^* to successively greater degrees because they raise the $\gamma/(\alpha + \gamma)$ temperature and thus $|\Delta G_v|$.

In an effort to compensate for the different effects of the various alloying elements upon $\gamma/(\alpha + \gamma)$ boundary, these data are replotted in Figure 13 as a function of ΔG_v. This approach is seen to rearrange the relative positions of the curves. All J_s^* *vs* temperature curves for Fe-C-X now lie to the left of the curve for the Fe-C alloy, including that for the Co alloy. Displacements to higher $|\Delta G_v|$ values are still observed to be associated with the austenite stabilizing elements, which are in turn associated with higher values of ε. Since ferrite formers tend to segregate more to grain boundaries during austenitization, the above observation cannot be explained by $\Delta\sigma_{\gamma\gamma}$; reduction in $\Delta\sigma_{\alpha\gamma}$ (coherent), not necessarily occurring in parallel, must also be involved.

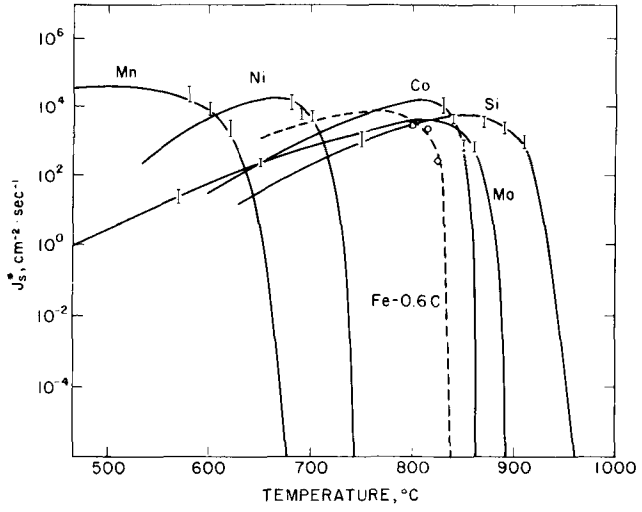

Fig. 12—Steady state nucleation rate, J_s^*, *vs* temperature in the alloys studied.

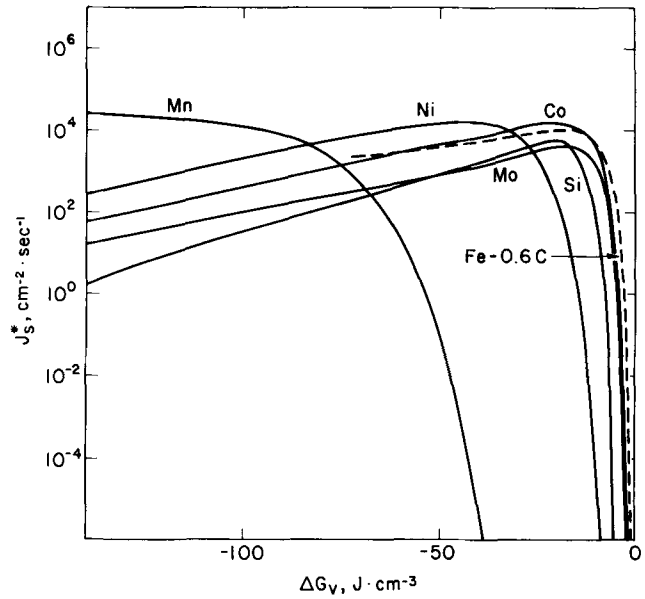

Fig. 13—Steady state nucleation rate, J_s^*, *vs* volume free energy change in the alloys studied.

VIII. THE ROLE OF J^* IN THE FORMATION OF A BAY IN THE TTT-DIAGRAM OF Fe-C-Mo ALLOYS

In Figure 14 the temperature dependence of J_s^* is compared with that of the parabolic rate constant, α, for ferrite growth[10] and the TTT curve for 1 pct transformation[10,11] in

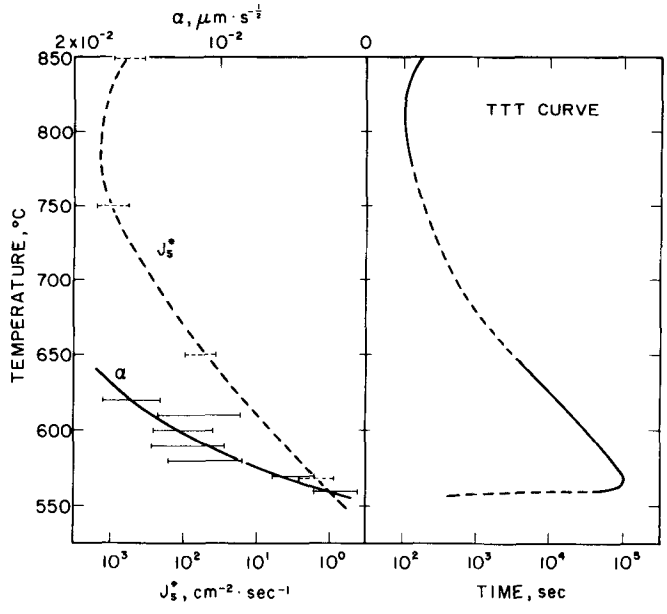

Fig. 14—Nucleation rate, J_s^*, and parabolic rate constant, α, *vs* temperature, and TTT-curve for 1 pct transformation in the Mo alloy studied.

the Fe-C-Mo studied during the present investigation. Earlier measurements on more dilute Fe-C-Mo alloys indicate that the α *vs* temperature curve is essentially a mirror image of the TTT-curve for the beginning of transformation;[8] the same situation is likely to obtain in the present alloy. However, unlike previous indirect estimates of J_s^* from α data and the Dubé[51] modification of the Johnson-Mehl equation,[52] which indicated that J_s^* is nearly independent of temperature in the bay region,[3] the present direct measurements of J_s^* show that it also varies with temperature in a manner parallel to that of the TTT-curve. Since it has long been recognized that overall transformation kinetics are more strongly affected by growth than by nucleation,[51,52,53] the earlier conclusion that the highly anomalous temperature dependence of α, which is ascribed to a solute drag-like effect,[3,8,14,15] is primarily responsible for the bay in the TTT-curve of this alloy seems to remain intact.

A more complete evaluation of the origin of the bay requires measurement of J^* and of α below as well as above the bay temperature in the same alloys. However, the severe degeneracy of the ferritic component of the microstructure in this region seriously interferes with the acquisition of both types of data.

IX. ON THE INFLUENCE OF GRAIN BOUNDARY STRUCTURE UPON NUCLEATION KINETICS

The low values of N found during the present investigation raise the same question as they did in the previous study on Fe-C alloys,[5] namely, whether or not a significant proportion of the nucleation occurs at relatively rare defects in the grain boundaries rather than at the average grain boundary structure. The commonly observed scatter in particle density from one grain boundary to the next is in the present context ascribed to ΔG^* values which vary with the identity of boundary planes and to the presence of $\{111\}_\gamma$ planes parallel to only a small minority of grain boundaries.[5] However, it is possible that such defects as ledges and intruder dislocations contribute to this scatter. The virtual impossibility of conducting TEM studies of the structure of austenite grain boundaries at which nucleation takes place because of the occurrence of the martensite transformation during quenching to room temperature was pointed out during the previous investigation.[5] In the present alloys, a further complexity arises from the varying extent to which each type of defect attracts X atoms. However, the greater reduction in ΔG^* attending the destruction of the austenite grain boundary rather than the strain field of an intruder dislocation or even the riser of a grain boundary ledge provides some measure of support for consideration of austenite grain boundaries as being characterized by an average energy during the nucleation process.

X. CONCLUSIONS

The nucleation kinetics of proeutectoid ferrite allotriomorphs at austenite grain boundaries in Fe-C-X alloys have been measured with recently improved experimental techniques.[5] Alloys containing about 0.5 at. pct C and 3 at. pct Mn, Ni, Si, or Co, and also an Fe-0.8 at. pct C-2.5 at. pct Mo alloy were studied. The accessible temperature range was 20° to 40 °C, except in the Fe-C-Mo alloy where it was an order of magnitude larger. The data acquired could be largely described in terms of a steady state nucleation rate characteristic of each alloy and reaction temperature. These data were analyzed on the basis of classical heterogeneous nucleation theory, using a pillbox model of the critical nucleus as was done in a previous study on Fe-C alloys.[5] Only a very small proportion of the austenite grain boundary area was again found to furnish viable nucleation sites.

Ortho- and paraequilibrium phase boundaries and volume free energy changes were calculated from the Hillert-Staffanson[21] regular solution model and the Lupis-Elliott[22,24] Central Atoms models. The Guttmann-McLean[44] noncompetitive sublattice model was employed to analyze the reduction in austenite grain boundary energy by segregation of substitutional alloying element.

The assumption that ferrite nuclei have the orthoequilibrium composition and evolve to critical nucleus size through the participation of boundary diffusion of alloying element gives a somewhat better accounting for the data in connection with the study on Fe-C alloys than either orthoequilibrium and volume diffusion transport of X or paraequilibrium and solute mass transport involving only carbon diffusion. In terms of the influence of alloying elements upon the volume free energy change and upon the interfacial energies, the observed characteristics of ferrite allotriomorph nucleation rates in the alloys studied may be summarized as follows:

1. Mn and Ni reduce the nucleation rate of grain boundary ferrite allotriomorphs primarily by reducing the volume free energy change during nucleation at a given reaction temperature. Mn further reduces the nucleation rate presumably through diminishing the austenite grain boundary energy more than the austenite:ferrite boundary energy.
2. Si increases nucleation kinetics because the more negative volume free energy change accompanying the marked increase in the $\gamma/(\alpha + \gamma)$ temperature more than offsets the decrease due to the reduction of the austenite grain boundary energy relative to that of the austenite:ferrite boundary energy.
3. Co has a weak effect on nucleation rates because it has only a minor influence on α-γ phase stability and a small tendency to segregate to austenite grain boundaries.
4. Mo increases the nucleation kinetics at high temperatures for the same reasons as Si. Extension of the measurements over a much wider temperature range shows a decrease in nucleation kinetics at lower temperatures. This decrease contributes substantially to bay formation in the TTT-curve for the beginning of transformation. However, the previously reported parallel diminution in growth kinetics continues to appear primarily responsible for the development of the bay.

ACKNOWLEDGMENTS

The authors wish to thank Professor J. K. Lee at Michigan Technological University, Houghton, MI for his discussion of the strain energy associated with precipitates, Dr. K. R.

Kinsman, formerly with the Scientific Laboratory of Ford Motor Company, Dearborn, MI for his cooperation in preparation of the Mn, Ni, Co, and Si alloys, and Dr. M. Semchyshen, Vice President (now retired) of Climax Molybdenum Co., Ann Arbor, MI, for preparation of the Mo alloy. They also express their appreciation to NSF for sponsorship of the research under Grant No. DMR-81-16905 from the Division of Materials Research.

REFERENCES

1. C. R. Simcoe, A. R. Elsea, and G. K. Manning: *Trans. AIME*, 1955, vol. 203, p. 193.
2. K. Mazanec and J. Cadek: *Rev. de Met.*, 1958, vol. 55, p. 501.
3. K. R. Kinsman and H. I. Aaronson: *Transformation and Hardenability in Steels*, Climax Molybdenum Company, Ann Arbor, MI, 1967, p. 39.
4. D. J. Swinden and J. H. Woodhead: *JISI*, 1971, vol. 209, p. 883.
5. W. F. Lange, III, M. Enomoto, and H. I. Aaronson: *Metall. Trans. A*, in press.
6. S. A. Saltykov: *Stereometric Metallography*, 2nd ed. (in Russian), Moscow, Metallurgizdat, 1958.
7. E. E. Underwood: *Quantitative Stereology*, Addison-Wesley, Reading, MA, 1970.
8. P. G. Boswell, K. R. Kinsman, G. J. Shiflet, and H. I. Aaronson: *Mechanical Properties and Phase Transformations in Engineering Materials—Earl R. Parker Symposium on Structure Property Relationships*, TMS-AIME, Warrendale, PA, 1986, p. 445.
9. G. J. Shiflet, H. I. Aaronson, and J. R. Bradley: *Metall. Trans. A*, 1981, vol. 12A, p. 1743.
10. G. J. Shiflet and H. I. Aaronson: *Metall. Trans. A*, in press.
11. F. G. Berry and R. W. K. Honeycombe: *Metall. Trans.*, 1970, vol. 1, p. 3279.
12. J. R. Bradley, T. Abe, and H. I. Aaronson: *Rev. Sci. Inst.*, 1982, vol. 53, p. 98.
13. W. F. Lange, III and J. M. Rigsbee: *Metallography*, 1980, vol. 13, p. 375.
14. J. R. Bradley and H. I. Aaronson: *Metall. Trans. A*, 1981, vol. 12A, p. 1729.
15. K. R. Kinsman and H. I. Aaronson: *Metall. Trans.*, 1973, vol. 4, p. 959.
16. K. C. Russell: *Phase Transformations*, ASM, Metals Park, OH, 1970, p. 219.
17. H. I. Aaronson and J. K. Lee: *Lectures on the Theory of Phase Transformation*, TMS-AIME, Warrendale, PA, 1975, p. 83.
18. M. Hillert: *ibid.*, p. 1.
19. R. K. Trivedi and G. M. Pound: *Acta Metall.*, 1967, vol. 15, p. 1761.
20. M. Enomoto and H. I. Aaronson: *Metall. Trans. A*, 1986, vol. 17A, pp. 1381-84.
21. M. Hillert and L-I. Staffanson: *Acta Chem. Scand.*, 1970, vol. 24, p. 3618.
22. C. H. P. Lupis and J. F. Elliott: *Acta Metall.*, 1967, vol. 15, p. 265.
23. E-H. Foo and C. H. P. Lupis: *Acta Metall.*, 1973, vol. 21, p. 1409.
24. J-C. Mathieu, D. Durand, and E. Bonnier: *J. Chim. Phys.*, 1965, vols. 11-12, p. 1289.
25. M. Enomoto and H. I. Aaronson: *CALPHAD*, 1985, vol. 9, p. 43.
26. B. Uhrenius: *Hardenability Concepts with Application to Steel*, TMS-AIME, Warrendale, PA, 1978, p. 28.
27. L. Kaufman and H. Nesor: *CALPHAD*, 1978, vol. 2, p. 55, p. 81, p. 117, p. 295, p. 325; *CALPHAD*, 1979, vol. 3, p. 45.
28. J. S. Kirkaldy, B. A. Thomson, and E. A. Baganis: *Hardenability Concepts with Applications to Steel*, TMS-AIME, Warrendale, PA, 1978, p. 82.
29. M. Enomoto, T. Tanaka, and H. I. Aaronson: unpublished research, National Research Institute for Metals, Tsukuba, Japan, and Carnegie-Mellon University, Pittsburgh, PA, 1983.
30. M. Hillert: *Phase Transformations*, ASM, Metals Park, OH, 1970, p. 181.
31. J. B. Gilmour, G. R. Purdy, and J. S. Kirkaldy: *Metall. Trans.*, 1972, vol. 3, p. 1455.
32. L. Kaufman, S. V. Radcliffe, and M. Cohen: *Decomposition of Austenite by Diffusional Processes*, John Wiley, New York, NY, 1962, p. 313.
33. G. Vander Velde, J. A. Velasco, K. C. Russell, and H. I. Aaronson: *Metall. Trans. A*, 1976, vol. 7A, p. 1519.
34. J. Fridberg, L. E. Torndahl, and M. Hillert: *Jernkontorets Ann.*, 1969, vol. 153, p. 263.
35. Y. W. Lee and H. I. Aaronson: *Acta Metall.*, 1980, vol. 28, p. 539.
36. M. R. Plichta, J. H. Perepezko, H. I. Aaronson, and W. F. Lange, III: *Acta Metall.*, 1980, vol. 28, p. 1031.
37. E. S. K. Menon and H. I. Aaronson: unpublished research, Carnegie-Mellon Univ., Pittsburgh, PA, 1984.
38. H. I. Aaronson and H. A. Domain: *Trans. TMS-AIME*, 1966, vol. 236, p. 781.
39. D. M. Barnett, J. K. Lee, H. I. Aaronson, and K. C. Russell: *Scripta Met.*, 1974, vol. 8, p. 1447.
40. K. C. Russell: *Acta Metall.*, 1969, vol. 17, p. 1123.
41. R. Defay and I. Prigogine: *Surface Tension and Adsorption*, John Wiley, New York, NY, 1966.
42. E. D. Hondros: in *Interfaces Conference—Melbourne*, Butterworths, Sydney, Australia, 1969, p. 77.
43. J. W. Gibbs: *The Scientific Papers of J. Williard Gibbs*, Dover, New York, NY, 1961, vol. 1, p. 219.
44. M. Guttmann and D. McLean: *Interfacial Segregation*, ASM, Metals Park, OH, 1979, p. 261.
45. M. Guttmann: *Surface Science*, 1975, vol. 53, p. 213.
46. M. Enomoto, C. L. White, and H. I. Aaronson: unpublished research, Carnegie-Mellon Univ., Pittsburgh, PA, 1980.
47. J. R. Bradley, Y. W. Lee, G. J. Shiflet, and H. I. Aaronson: unpublished research, Michigan Technological University and Carnegie-Mellon Univ., Pittsburgh, PA, 1979.
48. D. McLean: *Grain Boundaries in Metals*, Oxford, U.K., 1957, p. 133.
49. R. Hultgren, P. D. Desai, D. T. Hawkins, M. Gleiser, and K. K. Kelley: *Selected Values of the Thermodynamic Properties of the Elements*, ASM, Metals Park, OH, 1973.
50. C. S. Smith: *Trans. AIME*, 1948, vol. 175, p. 15.
51. C. A. Dubé: Ph.D. Thesis, Carnegie Institute of Technology, 1948.
52. W. A. Johnson and R. F. Mehl: *Trans. AIME*, 1939, vol. 135, p. 416.
53. J. W. Cahn: *Acta Metall.*, 1956, vol. 4, p. 449.